Accepted Manuscript

Improving the mechanical, thermal, dielectric and flame retardancy properties of cyanate ester with the encapsulated epoxy resin-penetrated aligned carbon nanotube bundle

Qingbao Guan, Li Yuan, Yi Zhang, Aijuan Gu, Guozheng Liang
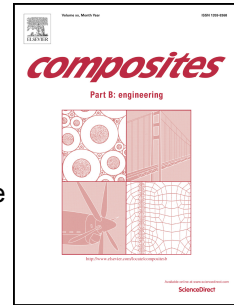
Please cite this article as: Guan Q, Yuan L, Zhang Y, Gu A, Liang G, Improving the mechanical, thermal, dielectric and flame retardancy properties of cyanate ester with the encapsulated epoxy resin-penetrated aligned carbon nanotube bundle, *Composites Part B* (2017), doi: 10.1016/j.compositesb.2017.05.029.

Improving the mechanical, thermal, dielectric and flame retardancy properties of cyanate ester with the encapsulated epoxy resin-penetrated aligned carbon nanotube bundle

Qingbao Guan, Li Yuan[∗],Yi Zhang, Aijuan Gu, Guozheng Liang

Jiangsu Key Laboratory of Advanced Functional Polymer Design and Application,

Department of Polymer Science and Engineering,

College of Chemistry, Chemical Engineering and Materials Science,

Soochow University, Suzhou, 215123, P.R. China

Abstract: Epoxy resins-penetrated aligned carbon nanotube bundles (ACNTB) microcapsules (ACNTB@EP MCs) and pristine ACNTB with porous structure were introduced into thermosetting cyanate ester (CE) resins to prepare high performance CE composites. Owing to the epoxy resins-penetrated ACNTB with significantly decreased defects and the chemical interaction at the interface of MCs and CE resin, CE with appropriated MCs shows better comprehensive performance than CE/ACNTB composite when the two composites contain the same amount of ACNTB. CE with 5 wt% MCs (CE/5MCs) shows the optimal flexural strength, impact resistance and tensile strength, which are 59%, 45% and 32% higher than that of CE, respectively. CE with 15wt% MCs (CE/15MCs) shows 24% higher in thermal conductivity, 35.1% lower in PHRR value than CE. CE/15MCs also exhibits the highest dielectric constant of 12.8–16.6 and a low dielectric loss of 0.022–0.066. The attractive performances of CE/MCs composites prove that the ACNTB@EP MCs are multi-functional fillers, which can simultaneously act as toughening agent, reinforcement while improving the thermal stability, flame retardancy and dielectric properties for high temperature

---

[∗] Corresponding author: Tel: +86 512 65880967;   fax: +86 512 65880089

E-mail address: yuanli@suda.edu.cn

thermosetting resins.

Keywords: particle-reinforcement; thermosetting resins; mechanical properties; thermal properties

1. Introduction

Cyanate ester (CE) resins are among the most important high performance thermosetting polymers, which can be used in the aerospace and microelectronic industry because of their highly desirable properties such as good radar transparency, low moisture absorption, excellent mechanical, thermal, and dielectric properties [1-5]. To meet the stringent requirements in the rapidly evolving high-tech area of aerospace, developing high performance CE-based composites with multifunctional properties including high self-healing ability, good flame retardancy and dielectric property have attracted much attention.

Previous studies showed that the incorporation of inorganic fillers into CE resins provides an efficient way to improve the integrated properties of the final products. The inorganic fillers included graphene oxide hybridized with manganese-schiff [6], glycidyl polyhedral oligomeric silsesquioxane [7], hexagonal boron nitride [8], organo-modified montmorillonite [9], layered silicates [10] or carbon nanotubes (CNTs) [11], etc. Among the inorganic fillers, CNTs were considered as the most versatile fillers for polymeric composites due to their unique combination of excellent mechanical, thermal and electrical properties. Moreover, their exceptional physical properties, including low density and high aspect ratio, made them ideal candidates for mechanical reinforcement of lightweight polymers [11-14]. The addition of functionalized multiwalled carbon nanotubes (MWCNT) significantly enhanced the flexural and impact strength of CE matrix and slightly increased the glass transition temperature (T_g) [15]. Dominguez *et al.* [16] reported that introducing 1 wt% MWCNT-containing

2

particles to oligomeric CE resulted in a 600% of increase in the storage modulus, 30 °C and 58 °C of increases in T_g and thermal stability, respectively. The reasons for improving the properties of CE using the above mentioned methods were mainly attributed to the good dispersion of inorganic particles and the strong interfacial interaction between fillers and matrices.

Although the addition of small amount of CNT to polymers could suppress the crack propagation within the matrix, it was completely ineffective for the existence of cracks. Many authors had noted that the encapsulated healing agents allowed polymers to exhibit excellent self-healing ability and improved toughness, resulting from the polymerization of the healing agent released to the crack surfaces and the crack blunting or crack bridging mechanism [17-22]. Then, the advantages of combining the healing agent-filled microcapsules (MCs) and CNT could endow polymer composites with superior integrated property.

Aligned carbon nanotube bundle (ACNTB) is composed of a number of CNTs that are joined end to end by van der Waals attractive force. They have a unique combination of high strength, stiffness, flexibility, strain to failure and conductivity, etc. [23-26]. However, ACNTB exhibits highly porous structures [27,28], the CNT joints and intertube interactions are weak and readily slipping between the CNTs. Therefore, the ACNTB cannot effectively transfer load and their strengths are rather lower than that of individual CNT [27,29,30]. It is more interesting to notice that the adhesive or polymer can penetrate into ACNTB and acts as an inter-bundle 'adhesive' to improve the CNT joints and intertube interactions, leading to better load transfer efficiency and higher strength of ACNTB [29-33]. Therefore, it is of great significance to design ACNTB-containing healing agents, which can be used as multifunctional fillers for

healing cracks within polymer matrix and improving thermal and mechanical properties of polymer composites.

The encapsulated epoxy resins-penetrated ACNTB (epoxy@ACNTB MC) has been synthesized in our laboratory and applied to CE resins to prepare self-healing systems [34], which show excellent self-healing ability and improved toughness. In present work, the effects of MCs on the properties of CE including flame retardancy, thermal, mechanical and dielectric properties are further investigated. For comparison, the ACNTB-based CE composites (CE/ACNTB) are also prepared with the content of ACNTB that is equal to that of CE/MCs system.

2. Experimental

2.1. Materials

Solid epoxy resin (diglycidyl ether of bisphenol A) with epoxide equivalent weight of 450-560 g/mol was purchased from Nantong Xingchen Synthetic Material Co. Ltd (China). Aligned carbon nanotube bundle (ACNTB) was purchased from Chengdu Organic Chemicals Co. Ltd, China (length: 30–100 μm). Modified amine curing agent (FS-2B), which could quickly initiate the curing reaction of epoxy resins at low temperature, was obtained from Chuzhou Huisheng Electronic Material Co. Ltd (China). Sodium dodecyl sulfate (SDS) used as a surfactant was purchased from Tianjin Chemical Regents Factory (China). Cyanate ester (CE) monomer was purchased from Yang Zhou Techia Chemical Co. Ltd (China). Diamino diphenyl sulfone (DDS) used as the catalyst for CE resin was obtained from Sinopharm Chemical Reagent Co. Ltd (China).

2.2. Preparation of the encapsulated epoxy resins-penetrated ACNTB

The preparation of the encapsulated epoxy resins-penetrated ACNTB (epoxy@ACNTB MCs) was prepared according to Ref. [34]. Epoxy resins (15 g) and

4

ACNTB (4.5 g) were mixed in acetone (200 ml) at 25 °C to obtain an epoxy resin-acetone solution containing ACNTB. When the solution became viscous and was degassed at 25 °C, 0.5 wt% SDS aqueous solution was added with stirring, then the suspension solution of epoxy@ACNTB was formed. Two hours later, epoxy@ACNTB particles became solid and could be easily separated from the aqueous solution. After washing with water, filtering, and freeze drying, epoxy@ACNTB particle powders were obtained. The epoxy@ACNTB particles were added into 0.5 wt% SDS aqueous solution (500 ml) with stirring for 20 min, followed by adding FS-2B (15 g). Stirring the mixture at 25 °C for 3 h, the black suspension was obtained. The suspension was washed using deionized water and filtered several times and then freeze dried for 24 h, and MCs were obtained. Fig. 1 shows the morphologies of ACNTB and epoxy@ACNTB MCs. The weight ratio of epoxy content to epoxy@ACNTB MCs was 74%, and the weight ratio of ACNTB to epoxy@ACNTB MCs was 14%. The T_{di} of the epoxy@ACNTB MCs was 266 °C.

2.3. Preparation of CE/epoxy@ACNTB MCs and CE/ACNTB systems

CE resin was heated to 130 °C, after melting to a clear liquid, 1 wt% DDS was added. The temperature of the mixture was raised to 145 °C and held at this temperature for 60 min with stirring. Then epoxy@ACNTB MCs were added to the mixture with stirring for 20 min. Afterward, the mixture was poured into a pre-heated mold for degassing at about 160 °C and cured as the following procedure: 160°C/2h+180°C/2h+200°C/2h. The relative weight contents of epoxy@ACNTB MCs to CE were 3, 5, 10 and 15 wt% and the resulting CE composites were designated as CE/3MCs, CE/5MCs, CE/10MCs and CE/15MCs, respectively. For comparison, 0.42, 0.7, 1.4 and 2.1 wt% pristine ACNTB, corresponding to the same content of ACNTB in CE/MCs, were added into CE to prepare CE/ACNTB composites using the same temperature program, and the

corresponding CE composites were designated as CE/0.42ACNTB, CE/0.7ACNTB, CE/1.4ACNTB and CE/2.1ACNTB.

2.4. Characterization

The morphology analysis of specimen was carried on using scanning electronic microscope (SEM, S-4700, HITACHI).

Flexural strength was measured according to GB/T 2567-2008 using a universal testing machine (KQL WDW100) at a cross-head speed of 10 mm/min.

Impact resistance test was measured according to GB/T 2567-2008 using a beam impact testing machine (XCJD-5J).

Tensile strength (σ) was measured according to GB/T 2567-2008 using a universal testing machine (KQL WDW100) at a cross-head speed of 5mm/min.

Fourier transform infrared (FTIR) spectra was obtained by scanning potassium bromide (KBr) discs of the samples using a FTIR spectrometer (Tensor 27, Bruker) to characterize the chemical structure. In order to monitor the cyanate ester (–OCN) group, the conversion (α) of –OCN was analyzed based on the FTIR data of CE systems before and after cure according to Eq.1 [35]. The vibration bands of –OCN at 2274/2238 cm^{-1} were chosen to calculate α of –OCN. The phenyl ring band at 1500 cm^{-1} was selected as the reference band.

$$\alpha = 1 - \left(\frac{\left(A_{-OCN} / A_{\text{phenyl ring}} \right)_{T,t}}{\left(A_{-OCN} / A_{\text{phenyl ring}} \right)_{T,t=0}} \right) \tag{1}$$

where A_{-OCN} and $A_{\text{phenyl ring}}$ were the areas of the bands of –OCN and phenyl ring, respectively, T and t were curing temperature and time, respectively.

Optical microscope (BK-POL, OPTEC) was used to investigate the distribution of fillers in the cured thin composite films.

Dynamic mechanical analysis (DMA, Q800, TA) was performed on samples using a

single cantilever beam clamping setup. DMA tests were carried out between 50–350 °C using a heating rate of 3 °C/min at 3Hz. Sample dimensions were $35mm \times 12mm \times 3mm$. The glass transition temperature (T_g) was determined from the peak temperature in the tan δ-temperature plot.

The thermal diffusivity was measured using a NanoFlash Thermal Diffusivity Meter (LFA 467, NETZSCH). Then the thermal conductivity was calculated from thermal diffusivity by Eq.2.

$$\lambda = \alpha \rho C_p \tag{2}$$

where λ was the thermal conductivity of the system, α was the thermal diffusivity of the system, ρ was the density, and C_p was the specific heat capacity under constant pressure.

Thermomechanical analysis (TMA, Q400, TA) was carried out within the range of 80–150 °C at a speed of 3 °C/min in a nitrogen atmosphere. The coefficient of thermal expansion (CTE) was calculated of using the following equation:

$$CTE = \frac{\Delta L}{L_0} \frac{1}{\Delta T} \tag{3}$$

where ΔL was the relative change in the length with respect to the initial length (L_0) of the sample when the temperature was increased by ΔT. Plotting the displacement as a function of the temperature, the values of $\Delta L/\Delta T$ were obtained from the slope of the linear fitting of the experimental data.

Oxygen index (LOI) was measured with an automatic oxygen index apparatus (LCK-09) according to GB/T 2406.2-2009. The dimensions of each sample were $110mm \times 6.5mm \times 3mm$.

The cone calorimeter test was performed on a FTT0007 Cone Calorimeter (FTT Company, England) according to ISO 5660 at an external heat flux of 35 kW/m². Each sample with a dimension of $110mm \times 100mm \times 3mm$ was put into an aluminum foil and

7

then put onto the specimen holder for testing.

The structure and morphology of residual chars were characterized using Raman spectra (HR-800, HORIBA JOBIN YVON) and stereo microscope (SZ780, OPTEC), respectively.

The dielectric property was measured using Novel Control Concept 80 (Germany) in the frequency range of $1-10^6$ Hz. Sample diameter was 20 mm and the thickness was 3.4 mm.

3. Results and discussion

3.1. Mechanical property of CE/ACNTB and CE/MCs composites

With the initial addition of individual ACNTB into CE, the mechanical properties of CE/ACNTB show a significant increase (Fig. 2). For instance, CE with 0.7 wt% ACNTB (CE/0.7ACNTB) exhibits the increase in flexural strength, impact resistance and tensile strength by 49%, 37% and 35%, respectively, as compared with pure CE resin. The incorporation of epoxy@ACNTB MCs into CE is more effective on improving mechanical property. In particular, CE/5MCs shows the optimal flexural strength, impact resistance and tensile strength that are 233 MPa, 19 KJ/m^2 and 42 MPa, which are 59%, 45% and 32% higher than that of CE, respectively. The increase in mechanical properties for CE/ACNTB and CE/MCs can be explained by the following reasons: (1) ACNTB has a unique combination of strength, stiffness, flexibility and porous structure that can be filled with epoxy or CE resin in CE composites. The resin penetrated-ACNTB shows better mechanical property than the pristine ACNTB [29,30], resulting in an increased mechanical property of CE composites; (2) ACNTB may break during the crack propagation, which can absorb energy and improve the mechanical property of CE composites; (3) ACNTB or MCs can pin or blunt the crack progress, thus absorbing energy and stabilizing the cracks in CE matrix [36,37].

The conversion of -OCN groups in CE-based composite is monitored to investigate the effect of polymer structure on the mechanical property. Apparently, the cure reaction in CE/MCs composites is more complete than that in CE/ACNTB as shown in Fig. 3, which is attributed to the catalytic effect of MCs on CE resin [34,38]. In present work, the epoxy-amine addition polymer shell of MCs can react with CE and effectively improve the dispersion of MCs in the matrix [34,39], resulting in the higher mechanical property of the matrix. Moreover, the aliphatic oxazolidinone rings, which can toughen CE matrix, can be formed by the reaction between –OCN group/triazine rings and a trace of epoxy resins that released from MCs during the cure process [13,34,40]. The FTIR of the region surrounding MCs in CE/MCs system shows the absorption peak of oxazolidinone rings at 1749 cm^{-1} (Fig. 4). This can indicate that MCs have good interface bonding with CE matrix and explain that CE/MCs composites show better mechanical property than CE/ACNTB, although both systems contain the same amount of ACNTB ($\leq$ 1.4 wt%) [39].

However, the mechanical properties of CE/ACNTB and CE/MCs start decreasing when the contents of ACNTB and MCs excess 0.7 wt% and 5 wt%, respectively. From Fig.5, it can be observed that as the fillers (ACNTB or MCs) increase, the distance between fillers and the dispersion of fillers in matrix decrease and the agglomeration of fillers gradually increases [41], thus the interface interaction between fillers and matrix decreases and the interaction among MCs increases [42]. When the higher filler content is applied, the interface interaction between fillers and matrix can be seriously weakened, the fillers cannot effectively transfer the load, and then the mechanical properties of CE with higher filler content decrease [42]. For CE/15MCs system, it shows the poorest mechanical properties. The shorter distance between MCs and the increase of MC agglomeration as shown in Fig. 5h can imply the increased interaction

among MCs and the decreased dispersion of MCs in the matrix, which lead to the decrease of mechanical property [39].

The improved mechanical properties of CE/ACNTB and CE/MCs are also evidenced by their SEM images of ductile impact fracture surfaces (Fig. 6). The cured CE resin shows a very smooth impact fracture surface, which is typical brittle fracture morphology of polymer. The impact fracture surfaces of CE/ACNTB and CE/MCs composites are much rougher than that of CE. The broken ACNTB and MCs, and the crack-pinning or crack-blunting phenomena at the vicinity of the crack path adjacent to ACNTB or MCs can be observed on the fracture surfaces of CE/ACNTB and CE/MCs composites.

3.2. Dynamic mechanical properties of CE/ACNTB and CE/MCs composites

The rigidity of materials is usually characterized by storage modulus [43]. As shown in Fig. 7A, the storage modulus of CE increases gradually with increasing the content of ACNTB that has high modulus [44]. During the fabrication of CE/ACNTB composites, CE resin penetrates inside the pores of ACNTB, forming CE polymer penetrated ACNTB, then the defects of ACNTB decrease and the strength of ACNTB is improved [29,30], which increase the rigidity of the CE/ACNTB composites. For CE/MCs composites, MCs can increase the storage modulus of CE for the penetrated ACNTB, but they also can decrease the storage modulus, owing to the presence of low-modulus epoxy resin core materials in MCs and the formation of aliphatic oxazolidinone rings. Therefore, CE/MCs composites exhibit a similar storage modulus value to CE below 150 °C regardless of the increase of MCs content (Fig. 7C). As the temperature continues to increase, the modulus of CE/MCs decreases. However, CE/MCs composites show higher modulus than CE between 150–250 °C probably due to the higher α of –OCN groups in CE matrix (Fig. 3B) and the high strength of ACNTB.

10

Because epoxy resin monomer core materials in MCs and the formed aliphatic oxazolidinone rings are less rigid than the triazine rings in matrix, CE/MCs composites show lower stiffness than CE/ACNTB composites.

DMA curve of pure CE resin (Fig. 7B) shows two tan δ maxima (T_{g1} and T_{g2}) implying the presence of a heterogeneous morphology of the cured network. The transition at low temperature (T_{g1} = 227 °C) is attributed to the cure reaction product formed by the reaction of CE resins and DDS [31], and the second transition occurs at around 292 °C (T_{g2}) corresponding to the polycyanurate [4]. For CE/ACNTB systems, the addition of ACNTB increases the T_{g1} of CE by 5–11°C for the restriction of ACNTB to the polymer chains. Because the dispersion of ACNTB in matrix become poorer with increasing ACNTB content (Fig. 5), CE with higher ACNTB content shows slightly lower T_{g1} than CE with lower ACNTB content [39,41]. The addition of ACNTB decreases the T_{g2} by 3-13 °C mainly for the lower conversion of -OCN groups (Fig. 3A) that disrupts the triazine rings crosslinked structure.

As the content of MCs increases, the T_{g1} of CE/MCs shows a gradually increasing trend resulting from the restriction of the increased MCs to the segmental motion of polymer chains and more complete conversion of -OCN groups in matrix (Fig. 3B). In particular, CE with 10-15 wt% MCs shows an increase of about 20 °C in T_{g1} than CE (Fig. 7D). The T_{g2} of CE/MCs shows a decreasing trend with the content of MCs, owing to the decreased rigid triazine rings and the formation of less rigid aliphatic oxazolidinone rings by the reaction between -OCN group/triazine rings and the released epoxy resins from MCs [13,34,40]. The addition of 15wt% MCs can decrease the T_{g2} value of CE to 256°C, being 36°C higher than that of CE. For the combined influences of the reasons caused higher T_{g1} and lower T_{g2} values of CE/MCs, two tan δ maxima eventually merge into single one when the content of MCs reaches 15 wt%, suggesting

11

that a more homogenous or better interfacial interaction system is obtained. For all CE composites, the T_{g2} decreases with increasing filler (ACNTB or MCs) content. The main reason is attributed to the fact that as the filler content increases, the interfacial areas between matrix and fillers increase, which can more seriously disrupt the rigid triazine ring structure in matrix.

3.3. Thermal conductivity of CE/ACNTB and CE/MCs composites

The thermal conductivity of composite is significantly affected by the thermal conductivity of filler and matrix, and the conductive channels. In present work, the content of filler is too low to form thermally conductive channels in the CE matrix. Because of the high theoretical thermal conductivity of CNT [45], the higher thermal conductivity of CE with ACNTB or MCs as shown in Fig.8 can be obtained. With the initial addition of MCs ($\leq$ 5 wt%), the thermal conductivity of CE/MCs is almost the same as that of CE/ACNTB due to their same amount of ACNTB. With respect to the high content of MCs ($\geq$ 10 wt%), the intermediate layer can be formed between stiff MCs and soft matrix, which alleviates the modulus mismatch between the fillers and matrix and decreases the thermal interfacial resistance. Xie *et al.* reported that a less stiff silica intermediate shell on the multi-walled carbon nanotubes played the same role in improving the thermal conductivity of the epoxy resin [46]. The thermal conductivity of CE/15MCs is 24% higher than that of CE. Additionally, improving the interfacial interaction between the fillers and polymer matrix is proven to be another effective factor on interfacial thermal conductivity enhancement [41,47]. CE/MCs (MCs $\geq$ 10 wt%) systems have stronger interfacial interaction than CE/ACNTB due to the chemical reaction between MCs and CE resin. Therefore, the CE/MCs systems exhibit better thermal conductivity than CE/ACNTB.

3.4. Coefficient of thermal expansion of CE/ACNTB and CE/MCs composites

The coefficient of thermal expansion (CTE) is a quantitative measurement of change in dimension with change in temperature, which is important in especially composite structures. The *ΔL/L* values of CE/ACNTB and CE/MCs composites in glassy state (80–150 °C) are shown in Fig. 9A. The CTE values of CE/ACNTB ($5.0–7.2\times10^{-5}$ °C^{-1}) and CE/MCs ($5.7–6.6\times10^{-5}$ °C^{-1}) were calculated based on Fig. 9A. The addition of pristine ACNTB with high thermal stability can decrease the CTE values of CE composites, however, the formation of crosslinked CE network is disrupted and the interfacial interaction between ACNTB and matrix is weak, which may increase the CTE of CE matrix. As a result, CTE values of CE/ACNTB composites show irregular change with the content of ACNTB (Fig. 9B). The decrease of CTE values in CE/MCs composites is attributed to the fact that the strong interaction between MCs and CE matrix. The interface layer between MCs and matrix can effectively transfer the heat to the MCs' core materials that can absorb energy and heat [48,49], thus decreasing the CTE of CE/MCs composites. As a result, the entire CE/MCs composites show lower CTE values than pure CE resin.

3.5. Flame retardancy of CE/ACNTB and CE/MCs composites

The limited oxygen index (LOI) is a measure of the percentage of oxygen that has to be present to support combustion of the polymer or composite. The higher the LOI, the lower the flammability is. The interaction between ACNTB and CE matrix is weak and the addition of ACNTB disrupts the formation of crosslinked CE network. It has been reported that the low crosslinking density of polymer can diminish the LOI [50-52]. For CE/ACNTB, the addition of ACNTB can slightly decrease the conversion (*α*) of –OCN groups in matrix (Fig.3A), which implies the decrease of chemical crosslinking density of CE matrix, and then the addition of ACNTB may reduce the LOI of CE matrix. But on the other hand, ACNTB has low flammability, which can improve the LOI of CE

matrix. Then the LOI of CE/ACNTB systems can be complicatedly influenced by ACNTB.

However, the LOI values of the whole CE/ACNTB systems are higher than that of pure CE resin (Fig. 10), resulting from the low flammability of ACNTB. In particular, CE/0.7ACNTB shows the highest LOI (29%) that is 6% higher than CE. During the combustion process, ACNTB can migrate towards the surface of the burning material, thus covering and shielding the underlying polymer [53] and reducing the flammability of composites. When the content of ACNTB reaches 1.4 wt%, the LOI values of CE/ACNTB decrease gradually, which is caused by the decreased α value (Fig. 3A) and the poorer dispersion of ACNTB in the CE matrix (Fig. 5c). The initial addition of MCs (3 wt%) enhances the LOI of CE to 28.9% owing to the existence of ACNTB and the increased α of -OCN groups (Fig. 3B). The LOI of CE/MCs starts decreasing when the content of MCs excesses 5 wt%, which is attributed to the increased aliphatic oxazolidinone rings, the reduced triazine rings in the system [13,34,40] and the decreased dispersion of MCs in matrix as well (Fig. 5) [54,55]. As the content of MCs further increases, the adverse influence of MCs on the LOI of CE/MCs gradually becomes a major factor, and then CE with 10–15wt% MCs may show lower LOI than CE.

Cone calorimeter is an effective technique to evaluate the flame retardancy of a material. The plots of heat release rate (HRR) of CE/ACNTB and CE/MCs composites as a function of time are shown in Fig. 11 and the typical cone calorimeter data are listed in Table 1. Combustion is a quite complex physical and chemical process determined by many factors such as viscosity and the structure of chars formed during combustion [56]. The HRR, especially the peak heat release rate (PHRR), has been found to be the most significant parameter to evaluate the fire safety [57]. The PHRR of

CE/ACNTB and CE/MCs are much lower than that of CE due to the presence of ACNTB. For the CE/ACNTB and CE/MCs composites, the presence of ACNTB increases the melt viscosity and promotes the formation of compact charred layers as heat barrier and thermal insulation [58], which reduces the PHRR values of CE composites. There is 39% reduction in PHRR value for CE/2.1ACNTB as compared with pure CE. The incorporation of MCs is more efficient to reduce PHRR, such as CE with only 3 wt% of MCs exhibiting a 30% lower in PHRR than CE. The further increase of MCs content does not result in a dramatic decrease in the PHRR value of CE/MCs. However, the average heat release rate (AHRR) and effective heat of combustion (EHC) values of CE/ACNTB and CE/MCs are about ~110 kW/m^2 and ~19.5 mJ/kg, respectively, which are similar to that of CE, indicating that the addition of ACNTB and MCs can only effectively suppress the combustion speed of CE composites.

The Raman spectra of residue chars of CE/ACNTB and CE/MCs composites after cone test show two big peaks at 1340 cm^{-1} and 1593 cm^{-1} (Fig.12), which are assigned to oriented graphitic (G peak) and disordered graphitic (D peak). The relative intensity ratio of D peak to G peak, I_D/I_G, reflects the degree of ordering of amorphous carbonaceous materials and microcrystalline planar size [59]. In present work, to accurately calculate I_D/I_G, the original curve is divided into peaks, and then the ratio of integral area of D peak to G peak is used to calculate I_D/I_G value. The charring residues of CE/ACNTB and CE/MCs composites exhibit greater I_D/I_G values than CE, implying more ordered amorphous carbonaceous materials and larger microcrystalline planar size [59]. The flame retardancy is improved through forming protective layers in the condensed phase and thus preventing the polymer from external radiation and heat feedback [60-63]. Eventually, the addition of MCs and ACNTB increases the flame

retardancy of CE composites, which is in a good agreement with the results of cone test.

Fig. 13 shows the stereo microscope images of residual chars of CE/ACNTB and CE/MCs composites. It can be observed from Fig. 13 that there are some light areas, which are caused by the light reflection from smooth compact charred layers or microcrystalline materials [64]. Apparently, CE/ACNTB and CE/MCs composites after combustion show increased compact charred layers or microcrystalline materials as compared to CE, indicating that CE/ACNTB and CE/MCs composites exhibit better flame retardancy than CE.

3.6 . Dielectric properties of CE/ACNTB and CE/MCs composites

Fig. 14 shows the dielectric properties of CE/ACNTB and CE/MCs composites as a function of frequency in a broadband $1-10^6$ Hz. The dielectric constants of CE/ACNTB and CE/MCs are higher than CE (3.34–3.59), which is due to the existence of ACNTB with high conductivity. When the two composites contain the same amount ACNTB, CE/MCs system shows higher dielectric constant than CE/ACNTB owing to the effective dispersion of MCs in matrix resulting from the chemical interaction between MCs and CE matrix. The dielectric losses of both composites are higher than that of CE mainly because of the interfacial polarization. CE/MCs system shows more stable dielectric loss than CE/ACNTB within a broad frequency range. Overall, the dielectric measurement results indicate that one can tailor the dielectric properties of CE composites by tuning the content of MCs. For instance, CE/15MCs shows the highest dielectric constant of 12.8–16.6 and a low dielectric loss of 0.022–0.066. Therefore, CE/MCs composites are also attractive for dielectric applications.

4. Conclusions

CE composites with epoxy@ACNTB MCs and pristine ACNTB were prepared. Because of the excellent mechanical property of ACNTB and the crack-pinning or

16

crack-blunting behaviors at the vicinity of the crack path adjacent to ACNTB or MCs, the addition of epoxy@ACNTB MCs and pristine ACNTB can improve the mechanical property of CE composites. CE/5MCs shows the optimal flexural strength, impact resistance and tensile strength, which are 59%, 45% and 32% higher than that of CE, respectively. The addition of ACNTB increases the storage modulus of CE, but MCs can effectively increase the lower T_g of CE composites. The addition of ACNTB and MCs also can increase the thermal conductivity and decrease the CTE values of CE mainly because of the presence of ACNTB with outstanding thermal conductivity and thermal stability property. CE/MCs and CE/ACNTB show better flame retardancy than CE mainly owing to the existence of ACNTB, which can significantly promote the formation of compact charred layers. CE/MCs and CE/ACNTB also exhibit higher dielectric property than CE for the presence of ACNTB. CE with 15 wt% MCs shows the highest dielectric constant of 12.8–16.6 and a low dielectric loss of 0.022–0.066. Overall, CE with appropriate content of MCs can show more excellent comprehensive performance than CE/ACNTB for the significantly decreased defects of ACNTB and the chemical interaction between MCs and CE matrix. Compared with traditional inorganic filler/CE composites, the present CE/MCs systems show a promising application in developing high performance self-healing composites with excellent mechanical, thermal and flame retardancy and dielectric properties.

Acknowledgements

References

[1] Hamerton I. Chemistry and technology of cyanate ester resins. Lodon: Chapman & Hall, 1994.

[2] Fang T, Shimp DA. Polycyanate esters: science and applications. Prog Polym Sci 1995; 20(1): 61-118.

[3] Ajaja J, Barthelat F. Damage accumulation in a carbon fiber fabric reinforced cyanate ester composite subjected to mechanical loading and thermal cycling. Compos Part B-Eng 2016;90(1):523-9.

[4] Nair CPR, Mathew D, Ninan KN. Cyanate ester resins, recent developments new polymerization techniques and synthetic methodologies. Adv Polym Sci 2001; 155: 1-99.

[5] Gu LC, Liang GZ, Shen YP, Gu AJ, Yuan L. Preparation of high k expanded graphite/$CaCuTi_4O_{12}$/cyanate ester composites with low dielectric loss through controlling the interfacial action between conductors and ceramics. Compos Part B-Eng 2014;58: 66-75.

[6] Gu X, Zhang ZJ, Yuan L, Liang GZ, Gu AJ. Developing high performance cyanate ester resin with significantly reduced postcuring temperature while improved toughness, rigidity, thermal and dielectric properties based on manganese-Schiff base hybridized graphene oxide. Chem Eng J 2016; 298(15): 214-24.

[7] Jiao J, Zhao LZ, Wang L, Lv PP, Cui YH, Wu GL. A novel hybrid functional nanoparticle and its effects on the dielectric, mechanical, and thermal properties of cyanate ester. Polym Compos 2016; 37 (7): 2142-51.

[8] Wu HC, Kessler MR. Multifunctional cyanate ester nanocomposites reinforced by hexagonal boron nitride after noncovalent biomimetic functionalization. ACS Appl Mater Inter 2015; 7: 5915-26.

[9] Wu GL, Cheng YH, Wang KK, Wang YQ, Feng AL. Fabrication and

characterization of OMMt/BMI/CE composites with low dielectric properties and high thermal stability for electronic packaging. J Mater Sci-Mater El 2016; 27(6): 5592-9.

[10] Li JP, He QH, Xu RF, Hu BX. Cyanate ester/functionalized silica nanocomposite: synthesis, characterization and properties. Chin J Chem 2015; 33: 1259-68.

[11] Ma PC, Siddiqui NA, Marom G, Kim JK. Dispersion and functionalization of carbon nanotubes for polymer-based nanocomposites: a review. Compos Part A-Appl S 2010; 41(10): 1345-67.

[12] Cadek M, Coleman JN, Ryan KP, Nicolosi V, Bister G, Fonseca A, Nagy JB, Szostak K, Beguin F, Blau WJ. Reinforcement of polymers with carbon nanotubes: the role of nanotube surface area. Nano Lett 2004; 4(2): 353-6.

[13] Zhang W, Shen L, Phang I, Liu T. Carbon nanotubes reinforced nylon-6 composite prepared by simple melt-compounding. Macromolecules 2004; 37(2): 256-9.

[14] Liu T, Phang I, Shen L, Chow S, Zhang WD. Morphology and mechanical properties of multiwalled carbon nanotubes reinforced nylon-6 composites. Macromolecules 2004; 37(19): 7214-22.

[15] Wang JH, Liang GZ, Yan HX, He SB. Mechanical and thermal properties of functionalized multiwalled carbon nanotubes/cyanate ester composite. Polym Eng Sci 2009; 49(4): 680-4.

[16] Dominguez DD, Laskoski M, Keller TM. Modification of oligomeric cyanate ester polymer properties with multi-walled carbon nanotube-containing particles. Macromol Chem Phys 2009; 210(20): 1709-16.

[17] Yang HI, Kim DM, Yu HC, Chung CM. Microcapsule-type organogel-based self-healing system having secondary damage preventing capability. ACS Appl Mater Int 2016; 8(17): 11070-5.

[18] Haghayegh M, Mirabedini SM, Yeganeh H. Microcapsules containing multi-functional reactive isocyanate-terminated polyurethane prepolymer as a healing agent. Part 1: synthesis and optimization of reaction conditions. J Mater Sci 2016; 51(6): 3056-68.

[19] Li CM, Tan JJ, Gu JW, Qiao L, Zhang BL, Zhang QY. Rapid and efficient synthesis of isocyanate microcapsules via thiol-ene photopolymerization in Pickering emulsion and its application in self-healing coating. Compos Sci Technol 2016; 123: 250-8.

[20] Gao L, He JL, Hu J, Wang C. Photoresponsive self-healing polymer composite with photoabsorbing hybrid microcapsules. ACS Appl Mater Int 2015; 7(45): 25546-52.

[21] Zhu DY, Rong MZ, Zhang MQ. Self-healing polymeric materials based on microencapsulated healing agents: From design to preparation. Prog Polym Sci 2015; 49-50: 175-220.

[22] Chen KL, Zhou SX, Yang S, Wu LM. Fabrication of all-water-based self-repairing superhydrophobic coatings based on UV-responsive microcapsules. Adv Funct Mater 2015; 25(7): 1035-41.

[23] Fujii S, Honda SI, Machida H, Kawai H, Ishida K, Katayama M, Furuta H, Hirao T, Oura K. Efficient field emission from an individual aligned carbon nanotube bundle enhanced by edge effect. Appl Phys Lett 2007; 90(15): 269-9.

[24] Jiang Q, Wang X, Zhu Y, Hui D, Qiu Y. Mechanical, electrical and thermal properties of aligned carbon nanotube/polyimide composites. Compos Part B-Eng 2014; 56: 408-12.

[25] Nam TH, Goto K, Yamaguchi Y, Premalal EVA, Shimamura Y, Inoue Y, Arikawa S, Yoneyama S, Ogihara S. Improving mechanical properties of high volume fraction aligned multi-walled carbon nanotube/epoxy composites by stretching and pressing.

Compos Part B-Eng 2016; 85: 15-23.

[26] Dalton AB, Collins S, Muñoz E, Razal JM, Ebron VH, Ferraris JP, Coleman JN, Kim BG, Baughman RH. Super-tough carbon-nanotube fibres. Nature 2003; 423(6941): 703.

[27] Miao M, McDonnell J, Vuckovic L, Hawkins SC. Poisson's ratio and porosity of carbon nanotube dry-spun yarns. Carbon 2010; 48(10): 2802-11.

[28] Jafari MS, Sobhani AB, Khoshkhahesh V, Taherpour A. Mechanical buckling of nanocomposite rectangular plate reinforced by aligned and straight single-walled carbon nanotubes. Compos Part B-Eng 2012; 43(4): 2031-40.

[29] Gspann TS, Montinaro N, Pantano A, Elliott JA, Windle AH. Mechanical properties of carbon nanotube fibres: St Venant's principle at the limit and the role of imperfections. Carbon 2015; 93: 1021-33.

[30] Peng B, Locascio M, Zapol P, Li S, Mielke SL, Schatz GC, Espinosa HD. Measurements of near-ultimate strength for multiwalled carbon nanotubes and irradiation-induced crosslinking improvements. Nat Nanotechnol 2008; 3(10): 626-31.

[31] Kwon CH, Chun KY, Kim SH, Lee JH, Kim JH, Lima LD, Baughman RH, Kim SJ. Torsional behaviors of polymer-infiltrated carbon nanotube yarn muscles studied with atomic force microscopy. Nanoscale 2015; 7(6) 2489-96.

[32] Miaudet P, Badaire S, Maugey M, Derre A, Pichot V, Launois P, Poulin P, Zakri C. Hot-drawing of single and multiwall carbon nanotube fibers for high toughness and alignment. Nano lett 2012 5(11) 2212-5.

[33] Liu K, Sun Y, Lin X, Zhou R, Wang J, Fan S, Jiang K. Scratch-resistant, highly conductive, and high-strength carbon nanotube-based composite yarns. ACS Nano 2010; 4(10)5827-34.

[34] Zhang Y, Yuan L, Su Y, Gu A, Liang G. Preparation and property of epoxy resins-penetrated aligned carbon nanotube bundle hybrid microcapsules for self-healing polymers. High Perform Polym DOI: 10.1177/0954008316645847

[35] Fang P, Chen Z, Zhang S, Wang S, Wang L, Feng J. Microstructure and thermal properties of ethylene-(vinyl acetate) copolymer/rectorite nanocomposites. Polym Int 2006; 55(3): 312-8.

[36] Brown EN, White SR, Scottos NR. Microcapsule induced toughening in a self-healing polymer composite. J Mater Sci 2004; 39(5): 1703-10.

[37] Brown EN, White SR, Sottos NR. Fatigue crack propagation in microcapsule-toughened epoxy. J Mater Sci, 2006; 41(19): 6266-73.

[38] Pan Y, Xu Y, An L, Lu H, Yang Y, Chen W, Nutt S. Hybrid network structure and mechanical properties of rodlike silicate/cyanate ester nanocomposites. Macromolecules 2008; 41(23): 9245-58.

[39] Gkikas G, Barkoula NM, Paipetis AS. Effect of dispersion conditions on the thermo-mechanical and toughness properties of multi walled carbon nanotubes-reinforced epoxy. Compos Part B-Eng 2012; 43(6):2697-705.

[40] Li X, Xia Y, Xu W, Ran Q, Gu Y. The curing procedure for a benzoxazine-cyanate-epoxy system and the properties of the terpolymer. Polym Chem 2012; 3(6): 1629-33.

[41] Patti A, Russo P, Acierno D, Acierno S. The effect of filler functionalization on dispersion and thermal conductivity of polypropylene/multi wall carbon nanotubes composites. Compos Part B- Eng 2016, 94:350-9.

[42] Bagheri R, Pearson RA. Role of particle cavitation in rubber-toughened epoxies: II. Inter-particle distance. Polymer 2000; 41(1), 269-76.

[43] Song YS, Youn JR. Influence of dispersion states of carbon nanotubes on physical

properties of epoxy nanocomposites. Carbon, 2005; 43(7): 1378-85.

[44] El-Hami K, Hami El A. Predicting the reliability of aligned carbon nanotube bundles in mechanical structures. Appl Mech Mater 2011; 146, 124-9.

[45] Tabkhpaz M, Shajari S, Mahmoodi M, Park DY, Suresh H, Park SS. Thermal conductivity of carbon nanotube and hexagonal boron nitride polymer composites. Compos Part B-Eng 2016, 100:19-30.

[46] Cui W, Du F, Zhao J, Zhang W, Yang Y, Xie X, Mai YW. Improving thermal conductivity while retaining high electrical resistivity of epoxy composites by incorporating silica-coated multi-walled carbon nanotubes. Carbon 2011; 49(2), 495-500.

[47] Yao YM, Zeng XL, Wang FF, Sun R, Xu JB, Wong CP. Significant enhancement of thermal conductivity in bioinspired freestanding boron nitride papers filled with graphene oxide. Chem Mater 2016; 80(10): 1357-9.

[48] Nai SML, Wei J, Gupta M. Improving the performance of lead-free solder reinforced with multi-walled carbon nanotubes. Mat Sci Eng A 2006; 423(1): 166-9.

[49] Isitman NA, Kaynak C. Nanoclay and carbon nanotubes as potential synergists of an organophosphorus flame-retardant in poly (methyl methacrylate). Polym Degrad Stabil 2010; 95(9): 1523-32.

[50] Liu H, Wang X, Wu D. Novel cyclotriphosphazene-based epoxy compound and its application in halogen-free epoxy thermosetting systems: Synthesis, curing behaviors, and flame retardancy. Polym Degrad Stabil 2014; 103(1):96-112

[51] Wang B, Zhou K, Wang L, Song L, Hu Y, Hu S. Enhancement on physical properties of flame retarded ethylene-vinyl acetate copolymer/ferric pyrophosphate composites through electron beam irradiation. Compos Part B-Eng 2012; 43(2):641-646.

[52] Zhao HB, Liu BW, Wang XL, Chen L, Wang XL, Wang YZ, A flame-retardant-free and thermo-cross-linkable copolyester: Flame-retardant and anti-dripping mode of action. Polymer. 2014; 55(10):2394-403.

[53] Lu H, Wilkie CA. Synergistic effect of carbon nanotubes and decabromodiphenyl oxide/Sb2O3 in improving the flame retardancy of polystyrene. Polym Degrad Stabil 2010; 95(4): 564-71.

[54] Montero B, Bellas R, Ramírez C, Rico M, Bouza R. Flame retardancy and thermal stability of organic–inorganic hybrid resins based on polyhedral oligomeric silsesquioxanes and montmorillonite clay. Compos Part B-Eng 2014; 63(63)67-76.

[55] Wang ZJ, Kwon DJ, Gu GY, Lee Wl, JK Park, DeVries KL, Park JM. Ablative and mechanical evaluation of CNT/phenolic composites by thermal and microstructural analyses. Compos Part B-Eng 2014; 60(2):597-602

[56] Ferrari AC, Basko DM. Raman spectroscopy as a versatile tool for studying the properties of grapheme. Nat Nanotechnol 2013; 8(4): 235-46.

[57] Ma H, Tong L, Xu Z, Fang Z. Synergistic effect of carbon nanotube and clay for improving the flame retardancy of ABS resin. Nanotechnology 2007; 18(37): 375602-9.

[58] Ye L, Wu Q, Qu B. Synergistic effects and mechanism of multiwalled carbon nanotubes with magnesium hydroxide in halogen-free flame retardant EVA/MH/MWNT nanocomposites. Polym Degrad Stabil 2009; 94(5): 751-6.

[59] Tuinstra F, Koenig JL. Raman spectrum of graphite. J Chem Phys 1970; 53(3): 1126-30.

[60] Song S, Ma J, Cao K, Chang G, Huang Y, Yang J. Synthesis of a novel dicyclic silicon-/phosphorus hybrid and its performance on flame retardancy of epoxy resin, Polym Degrad Stabil 2014; 99(13): 43-52.

[61] Huang N, Chen Z, Wang J, Wei P. Synergistic effects of sepiolite on intumescent flame retardant polypropylene. Express Polym Lett 2010; 4(12): 743-52.

[62] Song L, Wu K, Wang Y, Wang Z. Flammability and thermo-oxidative decomposition of epoxy resin containing ammonium polyphosphate and metallic oxide. J Macromol Sci A 2009; 46(3): 290-5.

[63] Bourbigot S, Le Bras M, Delobel R, Decressain R, Amoureux JP. Synergistic effect of zeolite in an intumescence process: study of the carbonaceous structures using solid-state NMR. J Chem Soc, Faraday Trans 1996; 92(1): 149-58.

[64] Elias M, de la Rie ER, Delaney JK, Charron E, Morales KM. Modification of the surface state of rough substrates by two different varnishes and influence on the reflected light. Opt Commun 2006; 266(2): 586-91.

Table 1. Typical cone calorimeter data of CE/ACNTB and CE/MCs systems

	CE	CE/ACNTB (wt%)				CE/MCs (wt%)			
		0.42	0.7	1.4	2.1	3	5	10	15
PHRR (kW/m^2)	347.3	301.0	264.3	251.3	213.1	242.3	257.5	243.9	225.3
AHRR (kW/m^2)	110.6	102.7	104.1	112.0	114.1	103.3	97.1	105.3	111.5
EHC (mJ/kg)	19.9	20.2	19.7	19.5	19.8	19.2	19.2	19.3	19.6
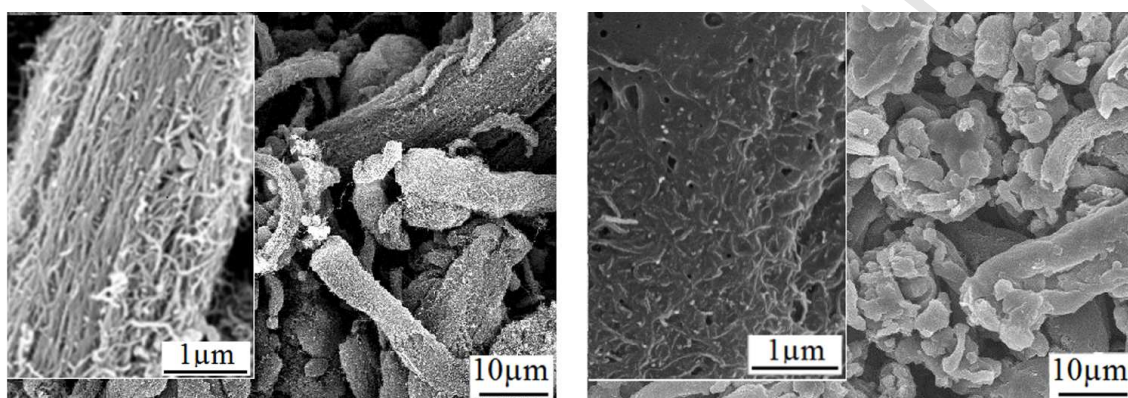
(a) ACNTB   (b) Epoxy@ACNTB MCs

Fig. 1 SEM images of ACNTB and epoxy@ACNTB MCs
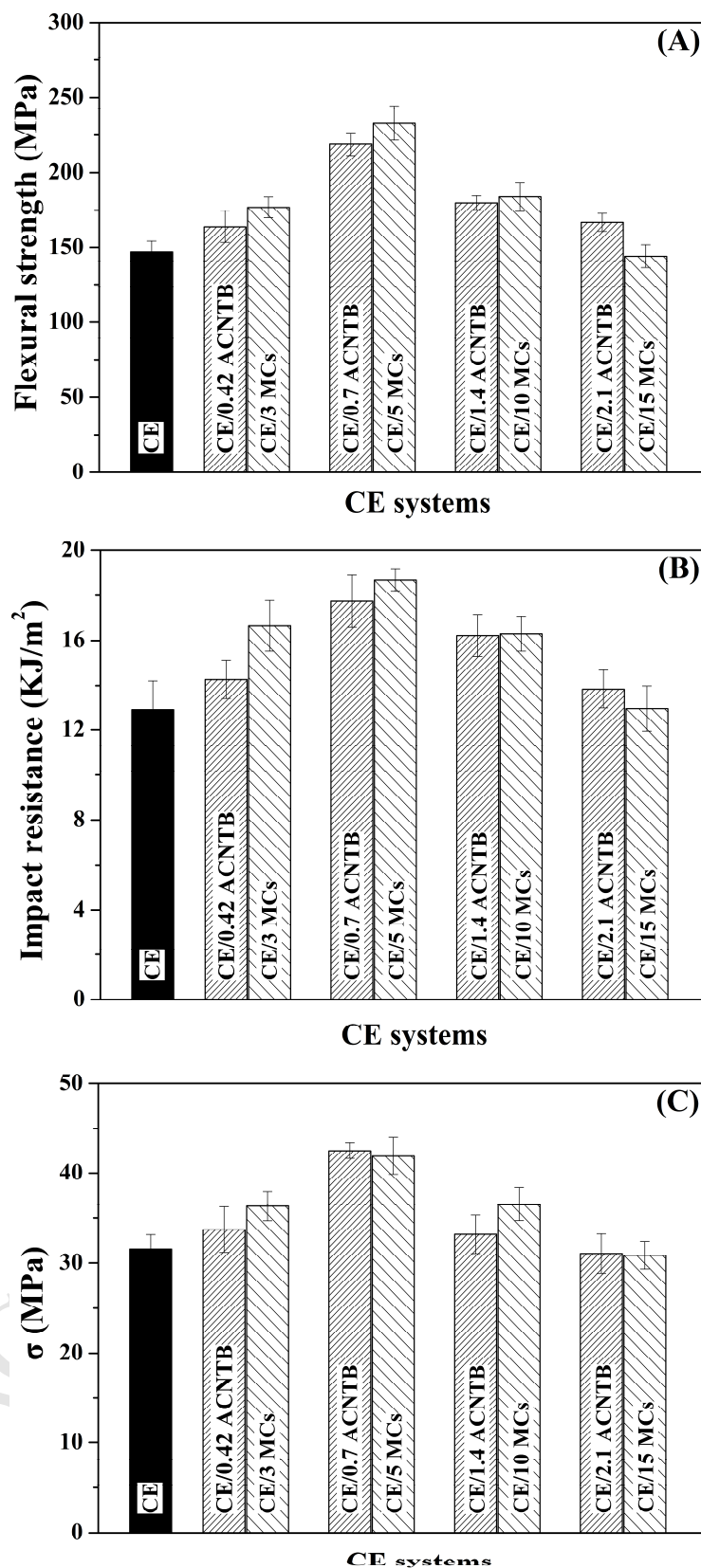
Fig. 2. Mechanical properties of CE/ACNTB and CE/MCs composites. (A) Flexural strength, (B) impact resistance and (C) tensile strength

27
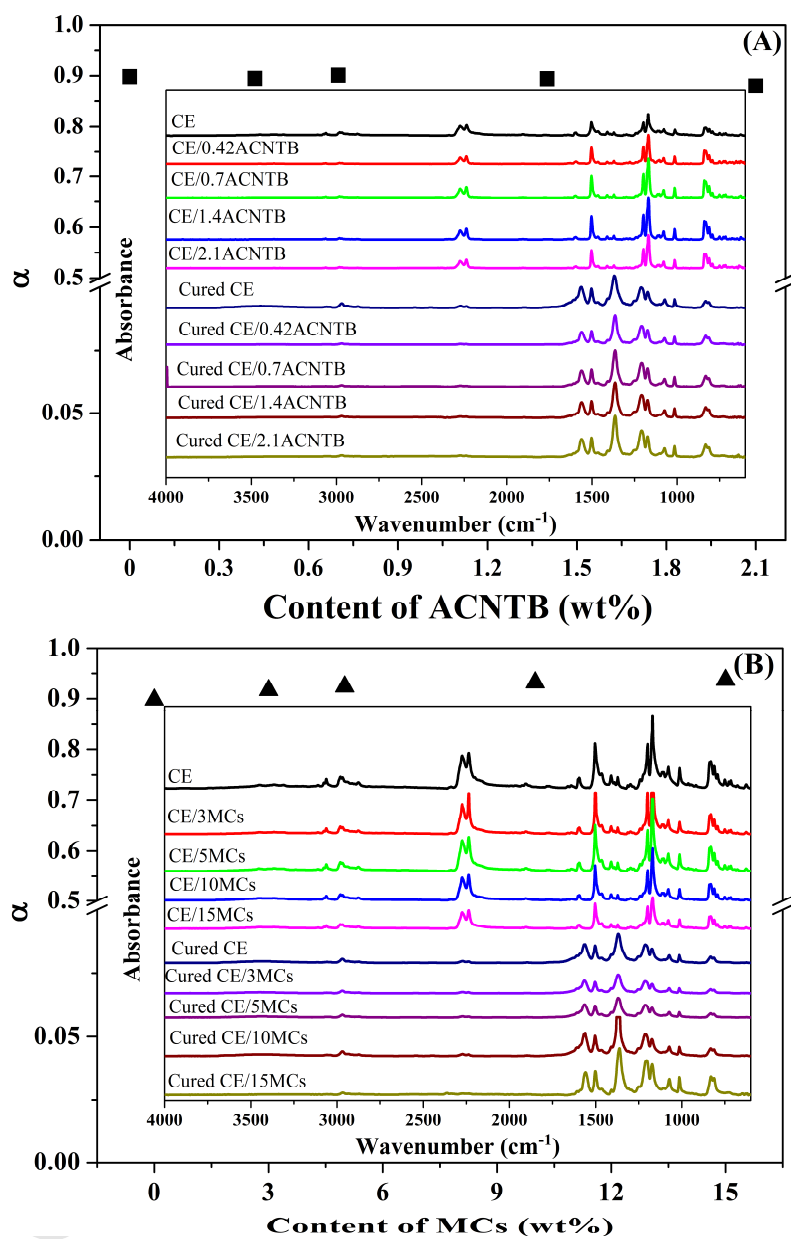
Fig. 3. Conversion (α) of -OCN groups in CE/ACNTB and CE/MCs composites along

with FTIR curves of CE/ACNTB and CE/MCs
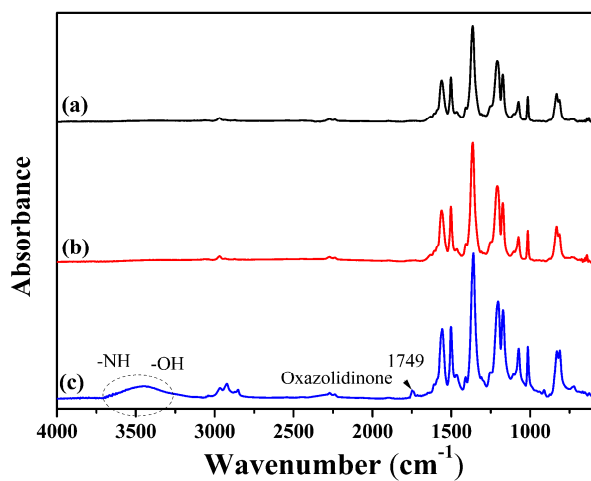
Fig. 4. FTIR curves of cured CE (a) and the region surrounding ACNTB in CE/ACNTB

(b) and the region surrounding MCs in CE/MCs system (c)

(a) CE/0.42ACNTB (b) CE/0.7ACNTB (c) CE/1.4ACNTB (d) CE/2.1ACNTB

(e) CE/3MCs (f) CE/5MCs (g) CE/10MCs (h) CE/15MCs
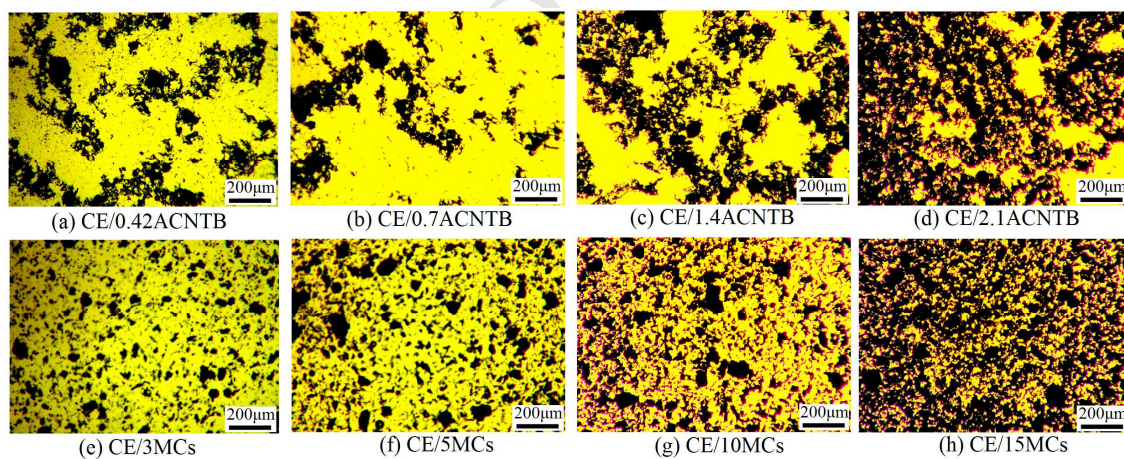
Fig. 5. Optical microscope images of the cured CE/ACNTB and CE/MCs thin films
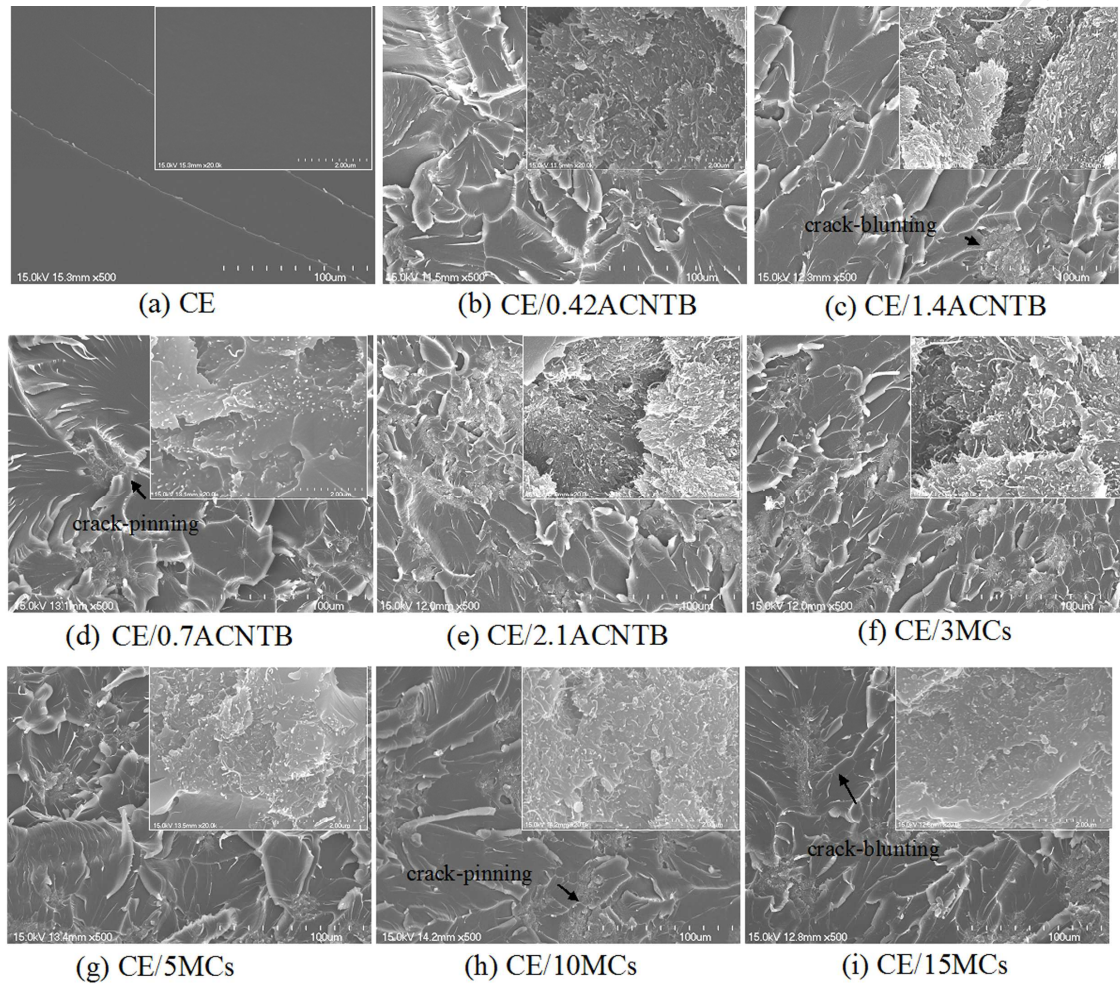
Fig. 6. SEM images of the fracture surfaces of CE/ACNTB and CE/MCs composites

after impact test
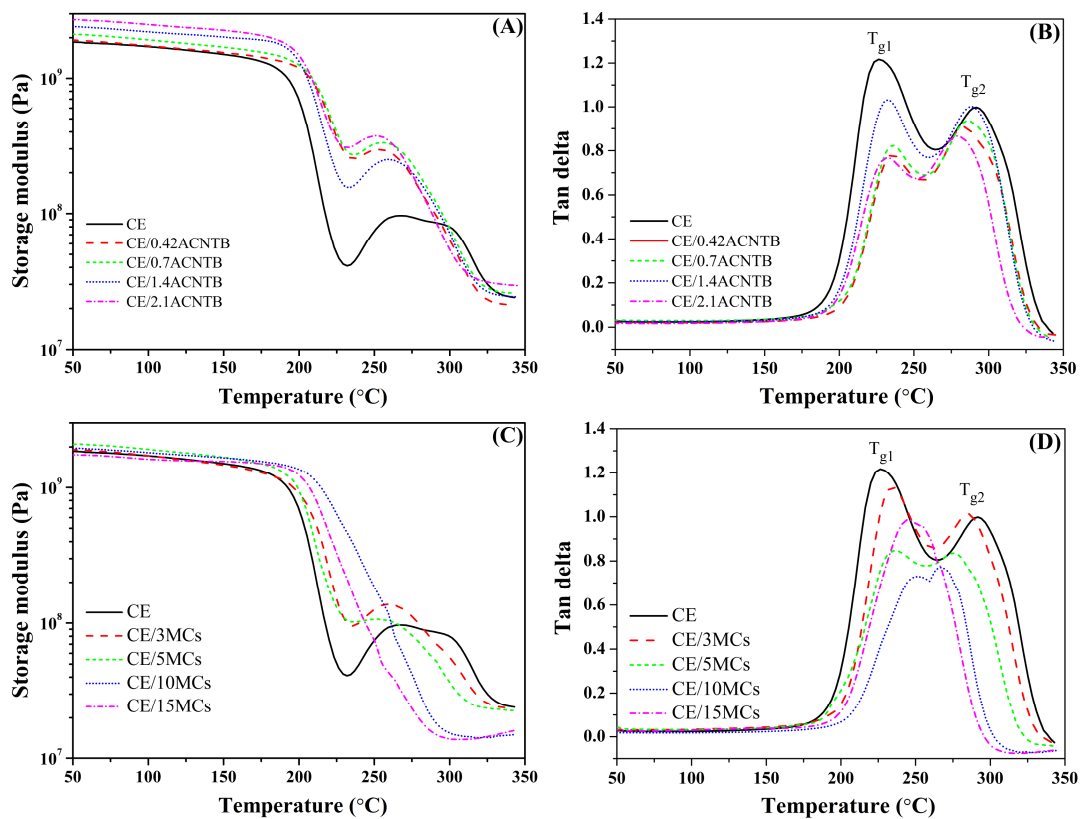
Fig. 7. Storage modulus and tan delta as a function of temperature for the CE/ACNTB

and CE/MCs composites
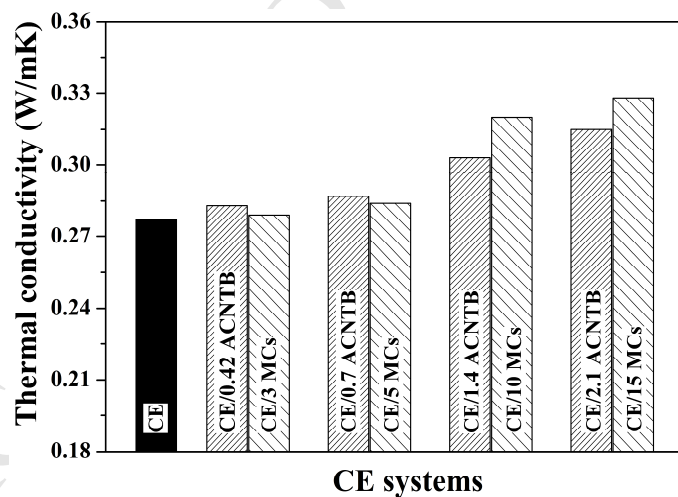
Fig. 8. Thermal conductivity of CE/ACNTB and CE/MCs composites
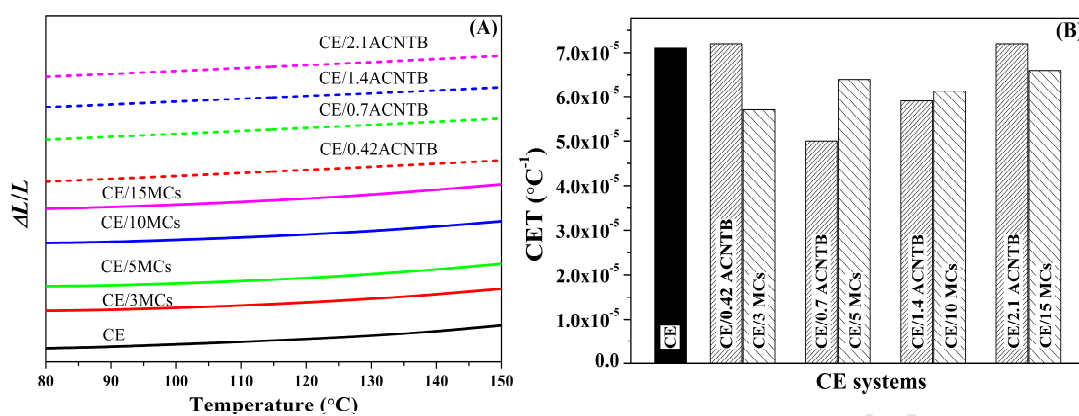
Fig. 9. *ΔL/L* values in glassy state (80–150 °C) (A) and CTE values (B) of CE/ACNTB

and CE/MCs composites
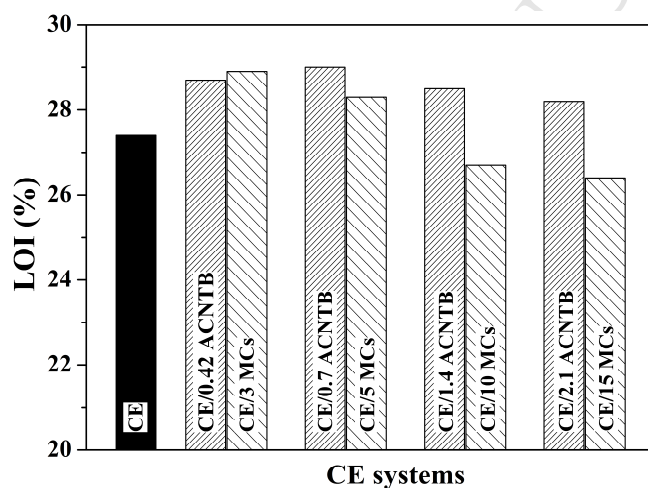
Fig. 10. Limited oxygen indexes of CE/ACNTB and CE/MCs composites

32
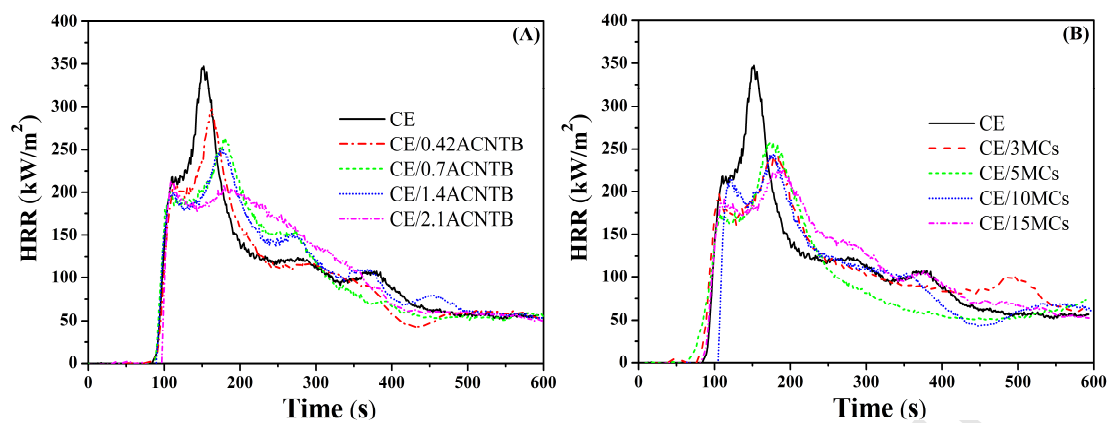
Fig. 11. HRR curves of CE/ACNTB (A) and CE/MCs (B) composites
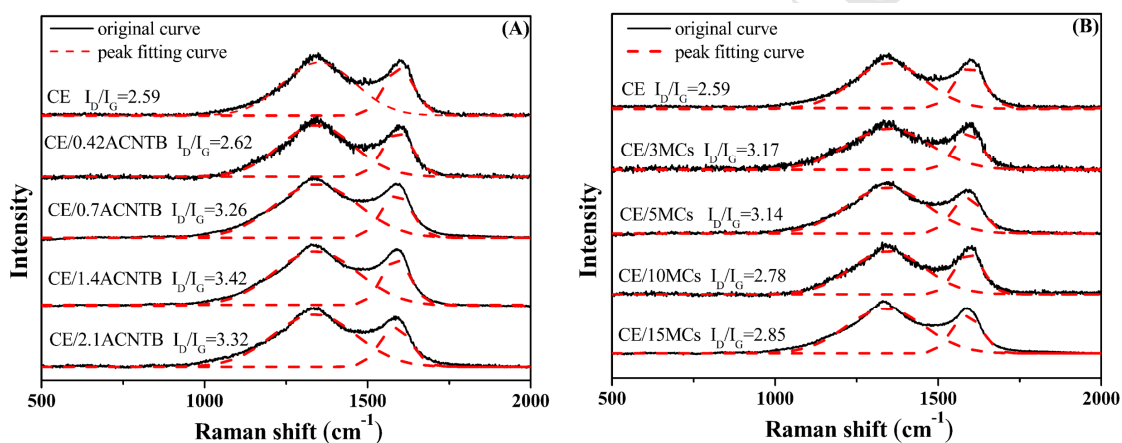
Fig. 12. Raman spectra of residue chars of CE/ACNTB (A) and CE/MCs (B) composites after cone test
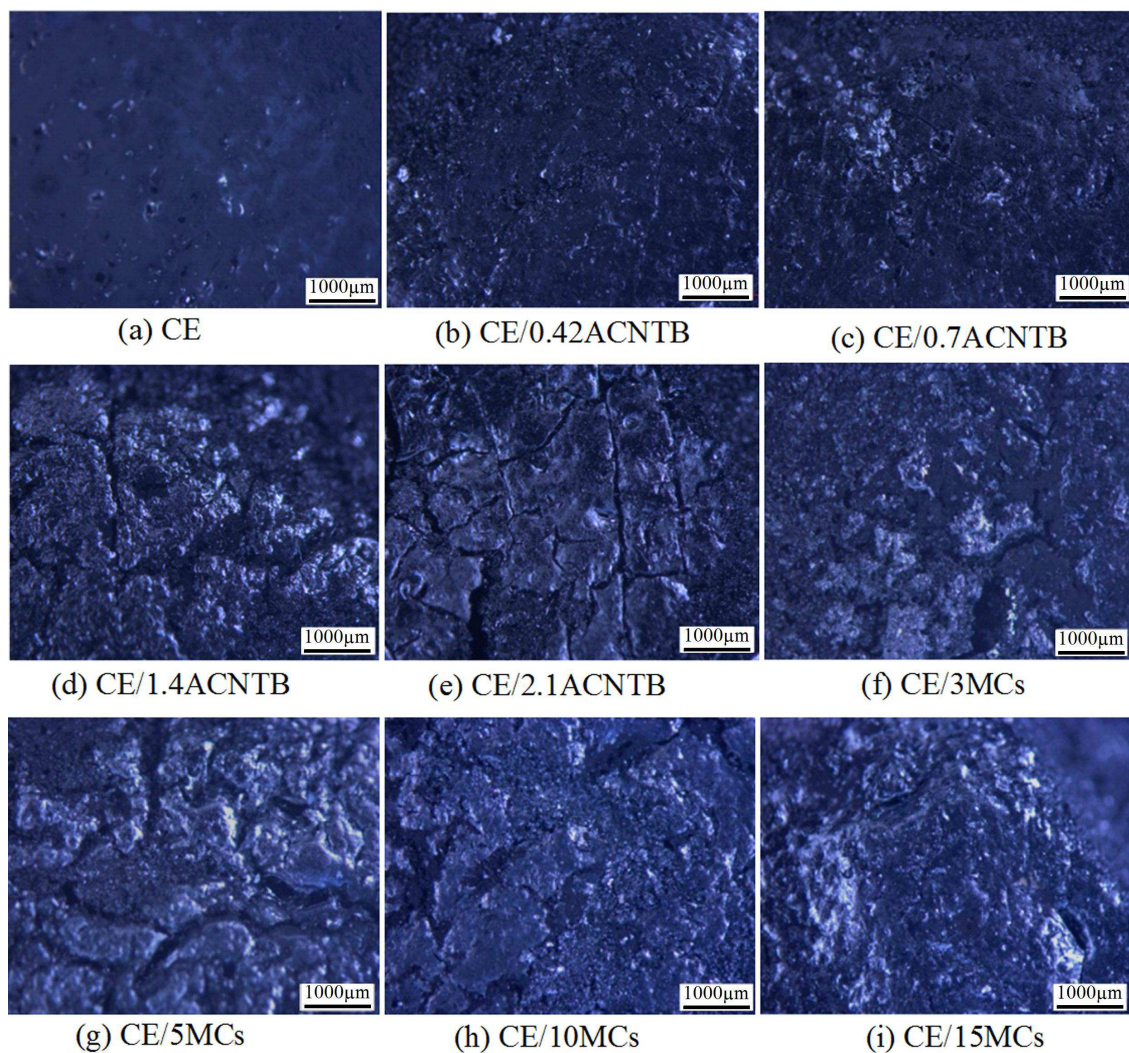
Fig. 13. Stereo microscope images of residual chars of CE/ACNTB and CE/MCs composites after cone test
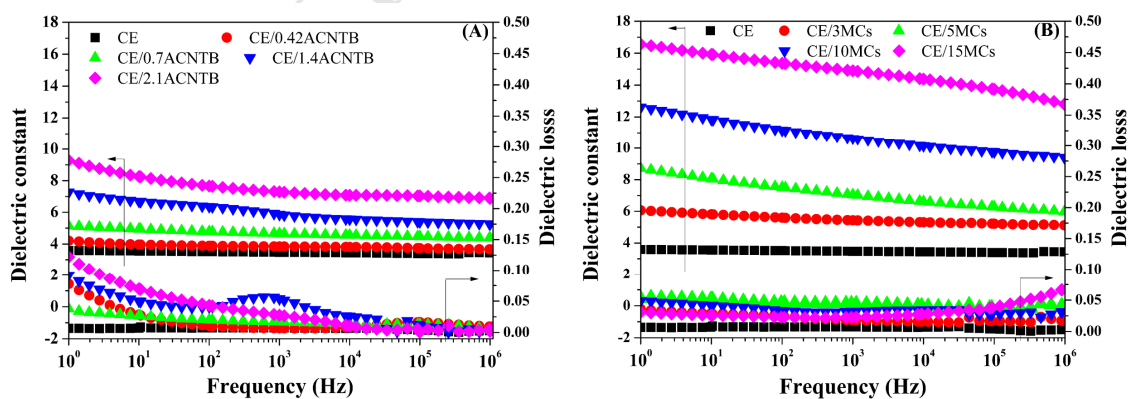
Fig. 14. Dielectric properties of CE/ACNTB (A) and CE/MCs (B) composites